EFFECT OF INITIAL CONDITIONS ON TURBULENT STRUCTURES OF VARIOUS SCALES IN A WAKE

Hui Li
Department of Mechanical Engineering, Kagoshima University
1-21-40, Korimoto, Kagoshima 890-0068, Japan
li@mech.kagoshima-u.ac.jp

Yu Zhou
Department of Mechanical Engineering, The Hong Kong Ploytechnic University
Hung Hom, Kowloon, Hong Kong, China
mmyzhou@polyu.edu.hk

ABSTRACT
The turbulent structures of various scales behind the solid and porous wake-generating bodies with the same characteristic dimension have been studies by the wavelet vector multi-resolution technique. Making a comparison of instantaneous sectional streamlines of various scales obtained with each wake generator, it is found that the behavior of large- and intermediate-scale structures in wakes depends on the initial conditions and the small-scale structures is independent of the initial conditions. The most significant contribution to Reynolds stress and turbulent energy appears to come from the large-scale and rib-like structures in the cylinder wake. In the screen wake, however, only the large-scale structure exhibits more contribution.

INTRODUCTION
It is well-known fact that the characteristics of the turbulent structure in the wake may differ as the wake-generating bodies or initial con ditions differ. A number of investigators (Screenivasan, 1981; Zhou and Antonia, 1994) have studied the effect of the initial conditions on the behaviour of a near turbulent wake. However, most of these investigations focus on organized structures, i.e. averaged large-scale structures, and clarify their contribution to turbulent transfer process behind various generators. It is difficult to deduce intermediate- and small-scale structures using the conventional techniques. As a result, until now there is a lack of information on the turbulent structures of various scales for different initial conditions.

In the past decade, there has been a growing interest in the use of wavelet analysis for turbulent flow data (Li, 1998). This technique allows time- and frequency-space analyses to be combined and produces a potentially clearer picture of time-frequency localization of turbulent structures. Li et al. (1999) applied the two-dimensional orthogonal wavelets to turbulent images for extracting the multi-resolution turbulent structures, however, few investigations concerned the extraction of turbulent structures in terms of time and scale from the measured velocity vector field. To solve this problem, Li and Zhou (2000) developed a new signal processing technique, i.e. wavelet vector multi-resolution analysis based on a two-dimensional orthogonal wavelet transform. This technique is unique that turbulent structures of different scales can be separated and characterised, and is reliably and effectively for analysis of multi-scale turbulent structures in time and frequency spaces.

The aim of the present work is to examine the turbulent structures of various scales behind different wake-generating bodies. The experimental methodology that is used consist in first extracting the turbulent structures of various scales by wavelet vector multi-resolution technique. The velocity vector field is decomposed in both Fourier and physical spaces, thus allowing the comparison of instantaneous sectional streamlines of various scales obtained with each wake generator. The contributions the various scale motions make to the Reynolds stress and the RMS vorticity have been quantified in each case.

TWO-DIMENSIONAL WAVELET VECTOR MULTI-RESOLUTION ANALYSIS
Let us consider a two-dimensional vector field $\vec{f}(x_1,x_2)$ and a two-dimensional orthogonal wavelet basis

$$\Psi_{m_1,n_1;m_2,n_2}(x_1,x_2)=2^{-(m_1+m_2)/2}\psi\left(2^{-m_1}x_1-n_1\right)\psi\left(2^{-m_2}x_2-n_2\right) \quad (1)$$

where $\psi(x)$ is an one-dimensional orthogonal wavelet basis.

The two-dimensional discrete vector wavelet transform is defined as

$$\overrightarrow{Wf}_{m_1,n_1;m_2,n_2}=\int_{-\infty}^{\infty}\int_{-\infty}^{\infty}\vec{f}(x_1,x_2)\Psi_{m_1,n_1;m_2,n_2}(x_1,x_2)dx_1dx_2 \quad (2)$$

The reconstruction of the original vector field can be achieved by using

$$\vec{f}(x_1,x_2)=\sum_{m_1}\sum_{m_2}\sum_{n_1}\sum_{n_2}\overrightarrow{Wf}_{m_1,n_1;m_2,n_2}\Psi_{m_1,n_1;m_2,n_2}(x_1,x_2) \quad (3)$$

The procedure of the wavelet vector multiresolution analysis can be summarised in two steps:

(1) Wavelet coefficients or wavelet spectrum of vector data is computed based on the discrete vector wavelet transform of Eq. (2).

(2) Inverse vector wavelet transform of Eq. (3) is applied to wavelet coefficients at each wavelet level, and vector components are obtained at each level or scale or in the wavelet spaces.

It is evident that a sum of all vector components in the wavelet spaces can reconstruct the original vector. The wavelet vector multi-resolution analysis may process fewer data by selecting the relevant details that are necessary to perform an extraction of the multi-scale structures and coherent structures, and decompose the vector data in both Fourier and physical spaces. The technique is unique in terms of its capability to separate turbulence structures of different scales. In this paper, we use the Daubechies family with index N=20, which is not only orthogonal, but also has smoothness and compact support, as the orthogonal wavelet basis.

EXPERIMENTAL SETUP

Experiments were carried out in a low turbulence wind tunnel with a 2.4 m long working section (0.35 m x 0.35 m). A circular cylinder and a screen of 50% solidity with the same height (h = 12.5 mm) were used and installed in the mid-plane and spanned the full width of the working section. Two orthogonal arrays (Fig.1), each of eight X-wires, were used. Eight X-wires were aligned in the (x, y)-plane, i.e. the plane of mean shear, and eight in the (x, z)-plane, which is parallel to both the cylinder axis and the streamwise direction. The sixteen X-wires allow velocity fluctuations u and v in the (x, y)-plane and u and w in the (x, z)-plane to be obtained simultaneously with a sampling frequency of f_s = 3.5 kHz. The nominal spacing between X-wires was about 5 mm. Measurements were made at x/h =20 and a constant free stream velocity (U_∞ = 6.7m/s). The corresponding Reynolds number Re was 5600.

INSTANTANEOUS TURBULENT STRUCTURES OF VARIOUS SCALES

In order to gain insight into the multi -scale turbulent structures, we apply wavelet vector multi-resolution analysis to the experimental velocity vector data of turbulent wakes.

The spanwise and lateral components of vorticity at each of the scales can be also defined in terms of the derivatives of the instantaneous velocity components $U_i = \overline{U} + u_i$, $V_i \cong v_i$ ($\overline{V} \cong 0$), and $W_i \cong w_i$ ($\overline{W} \cong 0$), where an overbar denotes time averaging and the index, i, stands for scale, respectively, viz.

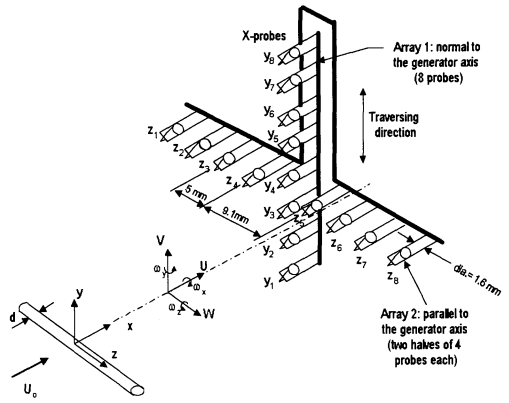

Figure 1: Experimental arrangement.

$$\omega_{zi} = \frac{\partial V_i}{\partial x} - \frac{\partial U_i}{\partial y} = \frac{\partial v_i}{\partial x} - \frac{\partial (\overline{U} + u_i)}{\partial y} \approx \frac{\Delta v_i}{\Delta x} - \frac{\Delta (\overline{U} + u_i)}{\Delta y}$$

$$\omega_{yi} = \frac{\partial U_i}{\partial z} - \frac{\partial W_i}{\partial x} = \frac{\partial u_i}{\partial z} - \frac{\partial w_i}{\partial x} \approx \frac{\Delta u_i}{\Delta z} - \frac{\Delta w_i}{\Delta x}$$

In above equations, $\Delta y \approx \Delta z$ ($\approx 5.0mm$) is spacing between two X-wires; $\Delta x = -U_c \Delta t$, where $\Delta t = 1/f_s$ and $U_c = 0.87 U_\infty$ (Zhou & Antonia 1992) is the average convection velocity.

Figure 2 shows the measured sectional streamlines in the cylinder and screen wakes in the (x, y)-plane. The flow direction is right to left. It is suggested that the cylinder and screen wakes have different geometrical characteristics of the vortex structure, e.g., shape, size, and spacing of the vortices. However, only the large-scale structures can be identified. However, it is difficult to identify the structures smaller than large-scale vortices in the measured streamlines (Fig.2) for both the cylinder and screen wakes. The measured velocity vector data were decomposed based on the wavelet vector multi-resolution analysis. Figures 3 and 4 show the decomposed sectional streamlines of the cylinder and screen wakes, which were calculated from the components of velocity vector for wavelet levels9 to 12 in the (x, y)-plane. The central frequencies are 109, 219, 438 and 875 Hz for the cylinder wake and 130, 260 and 510Hz for the screen wake, representing different scales of turbulence structures. As shown in Fig.3 (a), six vortical structures are easily extracted in the cylinder wake. These structures correspond quite well to the large-scale structures in Fig.2 (a), which occur at frequencies around the average frequency (108 Hz) of Karman vorticies. Figure 4(a) exhibits ten vortex pairs in the screen wake with the central frequency of 130 Hz. These structures also correspond quite well to the large-scale structures in Fig.2 (b), and their occurrence is rather periodical. They are apparently the uppermost and energy-containing structures. Making a comparison between the cylinder and screen wakes, the size of the large-scale structure in cylinder wake is larger than that in screen wake, and the vortices of screen wake exhibit the elliptical

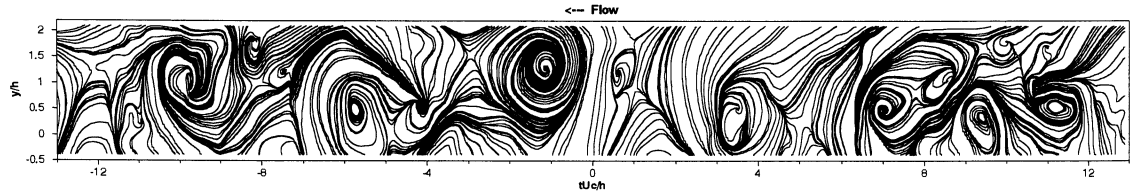

Figure 2(a): Measured cylinder wake.

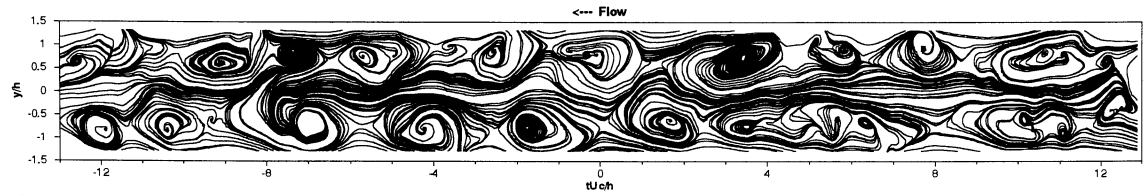

Figure 2(b): Measured screen wake.

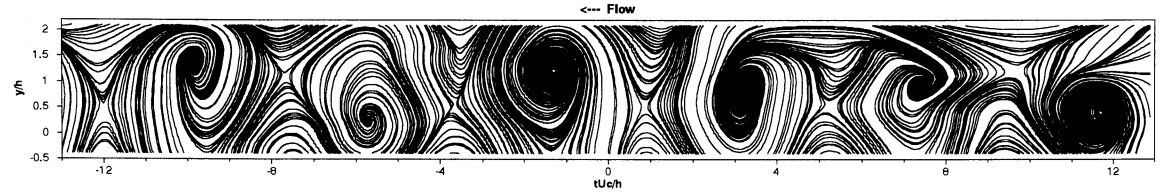

(a) f = 109 Hz

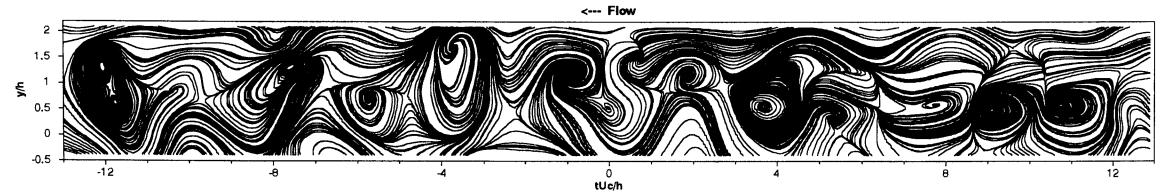

(b) f = 219 Hz

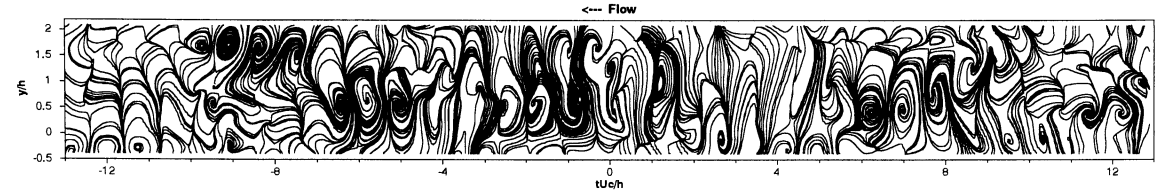

(c) f = 438 Hz

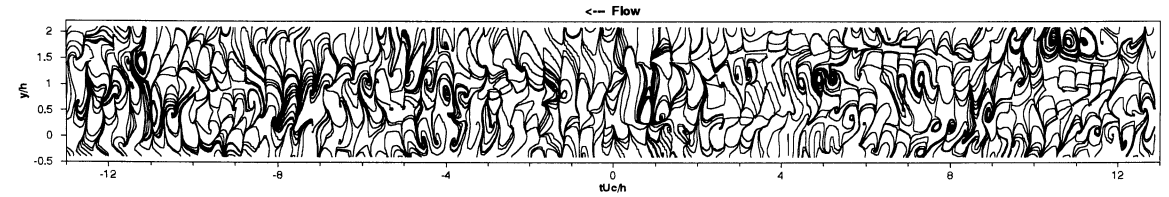

(d) f = 875 Hz

Figure 3: Instantaneous multi-scale streamlines of a cylinder wake in the (x, y)-plane.

shape. These differences reflect basic differences in the vortex formation mechanisms. Vortices in the circular cylinder wake are shed from the body surface, where those in the screen wake are likely to arise from instability in the developing mean wake profile.

The streamlines in Fig.3 (b), (c) and Fig.4 (b) show a number of structures that are smaller than those in Fig.3 (a) and Fig.4 (a). Some of them are the small vortices that are contained in vortical structures. Others correspond to the saddle regions between the vortices. It is evident that the intermediate-scale structures of screen wake exhibit periodical and their size are almost uniform. However, the structures of cylinder wake exhibit irregular shapes and various sizes. As the central frequency increases, as shown in Fig.3 (d) and Fig.4(c), a number of even smaller scale structures are identifiable. Their occurrence is rather periodical, and the structures of screen wake are similar to that of cylinder wake.

STATISTICAL ANALYSIS OF TURBULENT STRUCTURES OF VARIOUS SCALES

Reynolds Stresses of Various Scales

The lateral distributions of time-averaged shear stress components at different central frequency for the cylinder and screen wakes, which are normalized

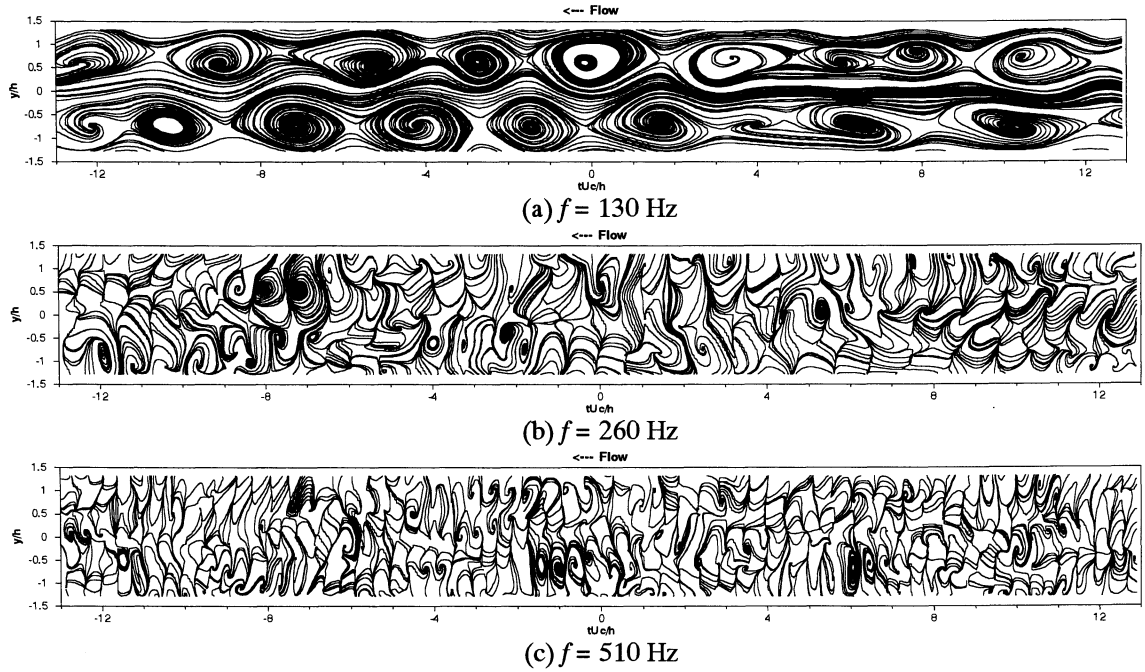

(a) f = 130 Hz

(b) f = 260 Hz

(c) f = 510 Hz

Figure 4: Instantaneous multi-scale streamlines of a screen wake in the (x, y)-plane.

by the maximum value of measured shear stress $\overline{uv}_{max}$, are shown in Fig.5. The distributions of $\overline{uv}/\overline{uv}_{max}$ component at each frequency are similar to that of the measured data for both of cylinder and screen wakes. The $\overline{uv}/\overline{uv}_{max}$ component decreases when increasing frequency, and varies greatly with the central frequency. For the cylinder wake, as shown in Fig.5 (a), $\overline{uv}/\overline{uv}_{max}$ component decreases rapidly with increasing the frequency in the range of high frequency ($f \geq 438Hz$). The $\overline{uv}/\overline{uv}_{max}$ component of 109 Hz remains everywhere largest in all components. The $\overline{uv}/\overline{uv}_{max}$ component of 219 Hz is also evidently larger than other components of $f \geq 438Hz$. This indicates that the contribution to the total shear stresses is greater from the large - and intermediate-scale structures. The peaks of $\overline{uv}$ components at 109 and 219 Hz appear around y/h = 1.0, which correspond to the averaged position of the vortex and saddle-point or rib-like structure. For the screen wake, $\overline{uv}/\overline{uv}_{max}$ component of 130 Hz remains everywhere largest in all components. Peaks of $\overline{uv}/\overline{uv}_{max}$ components at 130 Hz can be observed around y/h = 0.3. The maximum contribution to total $\overline{uv}$ is about 35% from the component of 130 Hz.

The distributions of time-averaged normal stress components $\overline{u^2}/\overline{u^2}_{max}$ at various frequency for the cylinder and screen wakes are plotted in Fig.6. The distribution of $\overline{u^2}/\overline{u^2}_{max}$ component at each frequency is similar to that of the total normal stress. In the case of the cylinder wakes, $\overline{u^2}/\overline{u^2}_{max}$ component decreases when increasing the central frequency. However $\overline{u^2}/\overline{u^2}_{max}$ component of 219 Hz is higher than that of 109 Hz in the range of $y/d <$ 0.7. This implies that the contribution to $\overline{u^2}/\overline{u^2}_{max}$ from the intermediate-scale structures is greater than that from large-scale structures due to the occurrence of the rib-like structures. For the screen wake, the component of $\overline{u^2}/\overline{u^2}_{max}$ around the average frequency of 130 Hz shows largest value. This indicates that the greatest contribution to the total normal stress comes from the component of large-scale structure in the screen wake.

From above results presented here, it can say that the most significant contribution to Reynolds stress and turbulent energy appears to come from frequency components of $f \leq 219Hz$, i.e. large-scale and rib-like structures, in the cylinder wake. However, in the screen wake, the contribution to Reynolds stress and turbulent energy comes from the large-scale structure. This would explain the significant difference between the wake of a porous body and that of a solid body.

Flatness Factor of Various Scales

Figure 7 illustrates the lateral distribution of flatness factor as a function of the central frequency for the cylinder and screen wakes. The measured flatness factor is also plotted in this figure. The frequency dependence of the flatness factor is evident. The distribution of flatness factor component at different frequency is similar to that of the measured data. The flatness factor components increase steadily with increasing y/h and increases more quickly in the

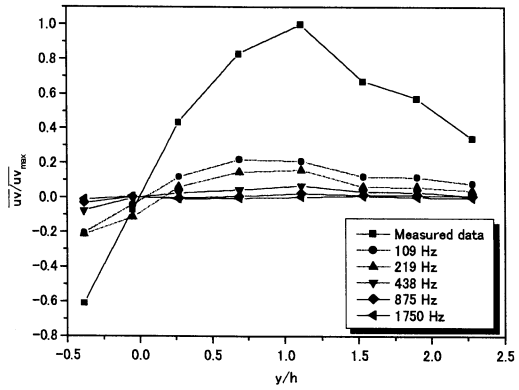

(a) Circular cylinder

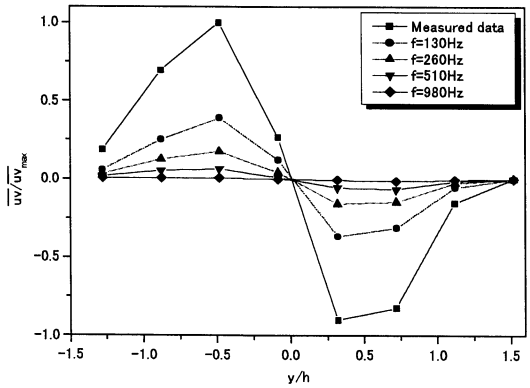

(b) Screen

Figure 5: Shear stress of various scales.

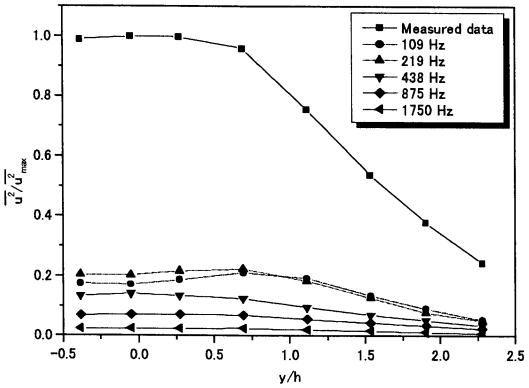

(a) Circular cylinder

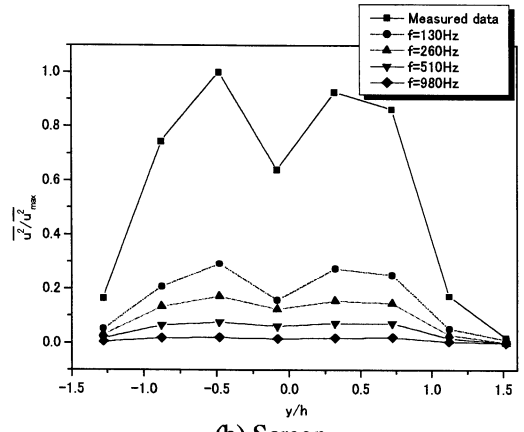

(b) Screen

Figure 6: Normal stress of various scales.

outer wake region. For cylinder wake, the flatness

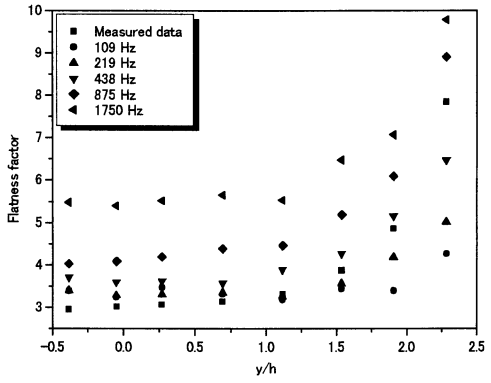

(a) Circular cylinder

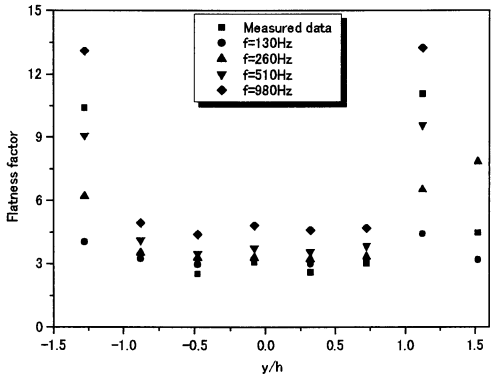

(b) Screen

Figure 7: Flatness factor of various scales.

factor of large- and intermediate-scale motions in the range of $f \leq 219$ Hz is close to the Gaussian value of 3 when $y/h < 1.5$, which is a direct consequence of local isotropy. For the screen wake, the flatness factor of $f \leq 260$ Hz is close to the Gaussian value of 3 as $|y/h| < 0.7$. As increasing frequency, the flatness factor begins to increase and a larger departure from the Gaussian value of 3 is observed at the central frequency of 980 Hz, since local isotropy is not valid for the small-scale motion. The flatness factor of cylinder wake is larger than that of screen wake in the centerline region at the higher central frequency. However, The flatness factor of cylinder wake becomes smaller than that of screen wake in the outer wake region. Although the measured flatness factor is close to the Gaussian value of 3 in the centerline region, the flatness factor component of high frequency exhibits a higher value. This implies that local isotropy is not expected to be valid when increasing frequency.

RMS Vorticity of Various Scales

In order to examine the dynamical role of various frequency components of vorticity, the lateral distribution of RMS value of vorticity components $\overline{\omega_z^2}$, which is normalized by the maximum value of measured vorticity $\overline{\omega_z^2}_{\max}$, is plotted as a function of the central frequency in Fig. 8. It is found that the variances of RMS vorticity components with y/h are

qualitatively similar to the measured RMS value of vorticity for $f \geq 438Hz$. The lateral variation of RMS vorticity components within range of $f \leq 219Hz$, however, decreases monotonically towards the edge of the wake, which is different from the measured RMS value of vorticity. When increasing the central frequency, the $\overline{\omega_z^2}/\overline{\omega_z^2}_{\max}$ first increases up to a maximum at f = 875 Hz, and then decreases. The value of $\overline{\omega_z^2}/\overline{\omega_z^2}_{\max}$ at f = 875 and 510 Hz almost exhibits the largest everywhere for the cylinder and screen wakes, respectively. The peak of $\overline{\omega_z^2}/\overline{\omega_z^2}_{\max}$ appeared in the total RMS value of vorticity results from the vorticity components of $f \geq 260Hz$, i.e. the small-scale structure.

In the case of cylinder wake, as shown in Fig.8 (a), the smallest value of the RMS vorticity component of f = 109 Hz indicates that the large-scale motion exhibits less contribution to the total RMS vorticity than other components. However, the RMS vorticity component of f = 219 Hz is slightly larger than that of f = 1750 Hz and is close to that of f = 438 Hz in the centerline region. This is due to the contribution from the rib-like structures in intermediate-scale motion.

For the screen wake, the RMS vorticity component of f = 130 Hz exhibits the largest value and more contribution to the total RMS vorticity near the centerline, although the RMS vorticity component of f = 510 Hz gives the largest value in the other region. The $\overline{\omega_z^2}/\overline{\omega_z^2}_{\max}$ components of screen wake decrease quickly towards the edge of the wake and their contribution to the total RMS vorticity is also less than that of the cylinder wake. These differences between the cylinder and screen wakes reflect basic differences in the vortex formation mechanisms. However, the RMS vorticity component of high frequency gives much more contribution to the total RMS vorticity everywhere for both of the cylinder and screen wakes.

CONCLUSIONS

(1) The behavior of large- and intermediate-scale structures in wakes depends on the initial conditions. However, the behavior of small-scale structures is independent of the initial conditions.

(2) The most significant contribution to Reynolds stress and turbulent energy appears to come from the large-scale and rib-like structures in the cylinder wake. In the screen wake, however, only the large-scale structure exhibits more contribution.

(3) The large-scale motion of the cylinder wake exhibits less contribution to the total RMS vorticity. However, the large-scale motion of the screen wake appears more contribution to the total RMS vorticity near the centerline.

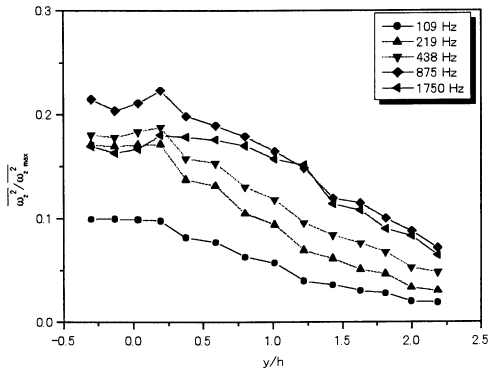

(a) Circular cylinder

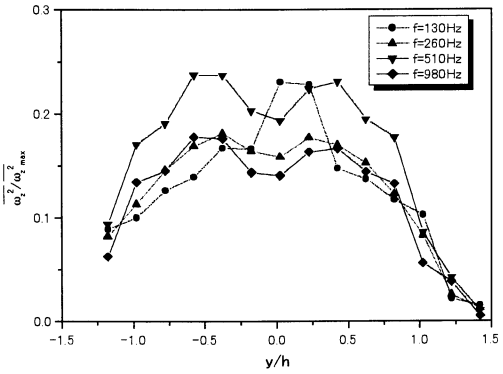

(b) Screen

Figure 8: RMS vorticity of various scales.

REFERENCES

Li, H., 1998, "Identification of Coherent Structure in Turbulent Shear Flow with Wavelet Correlation Analysis", ASME Journal of Fluids Engineering, Vol. 120, pp.778-785.

Li, H., Takei, M., Ochi, M., Saito, Y., and Horii, K, 1999, "Application of Two-dimensional Orthogonal Wavelets to Multi-resolution Image Analysis of a Turbulent Jet", Transactions of the Japan Society for Aeronautical and Space Sciences, Vol. 42, pp.120-127.

Sreenivasan, K. R., 1981, "Approach to Self-Preservation in Plane Turbulent Wakes", AIAA Journal, Vol.19, pp.1365-1367.

Zhou, Y., and Antonia, R.A., 1992, "Convection Velocity Measurements in a Cylinder Wake", Experiments in Fluids, Vol. 13, pp.63-70.

Zhou, Y., and Antonia, R.A., 1994, "Effect of Initial Conditions on Vortices in a Turbulent Near Wake", AIAA Journal, Vol. 32, pp.1207-1213.